EUROPEAN JOURNAL OF MATERIALS SCIENCE AND ENGINEERING
Volume 4, Issue 2, 2019: 53-60 | www.ejmse.tuiasi.ro | ISSN: 2537-4338

EJMSE

DOI: 10.36868/ejmse.2019.04.02.053

FATIGUE AND FRACTURE BEHAVIOR OF LPBF MANUFACTURED ALUMINUM ALLOY

Luke SUTTEY, Vadiraja SUDHAKAR*

Montana Technological University, Butte, MT 59701, USA

Abstract

Fatigue and fracture behavior of laser powder bed fusion (LPBF) processed aluminum alloy (AlSi10Mg) was evaluated in this investigation. High cycle fatigue and fracture characteristics were evaluated as a function of as-built specimen orientations and energy densities, used during processing. Fatigue tests were carried out on a rotating beam fatigue tester. Fracture characteristics were determined using SEM. Results indicate that aluminum alloy produced at 90° build angle orientation exhibited higher fatigue strength/life in comparison to the rest of build angle orientations. Higher fatigue strength and tensile toughness were observed for the specimens produced with relatively higher energy density at 49.9 J/mm^3. SEM investigations revealed ductile fracture surface features for specimens produced with higher energy density.

Keywords*: AlSi10Mg alloy, laser additive manufacturing, high cycle fatigue, S-N curves, fracture.*

Introduction

It is well-known that the additive manufacturing involving laser powder bed fusion (LPBF) processing can produce complex parts with greater dimensional accuracy [1]. In powder bed fusion method of LAM, the metal powder layer is spread uniformly on a build metal plate using a roller to produce an average layer bed thickness of 30-40 μm. This is followed by exposing the deposited powder layer to the laser in the desired pattern at scan speeds up to about 15m/s and the melting of the localized metal powder bed layer is facilitated by choosing an appropriate level of laser energy and laser scan speed [2]. The presently investigated aluminum alloy is popularly used in many engineering industries because of its unique combination of mechanical properties [3, 4]. Higher solidification rates that are typical of LAM/LPBF process, result in complex but very fine microstructures leading to improved mechanical properties [5]. However, the LPBF processing of aluminum alloys is difficult because of alloy's inherent characteristics that potentially lead to higher possible solidification defects in the product [6]. Because of this, many investigations have been aimed at producing denser parts typically varying laser power energy and scan speeds [7]. The currently used aluminum alloy has popular commercial uses for making aluminum castings with composition closer to eutectic composition (12.5% Si), providing unique properties [8, 9]. High porosity is known to be a major concern especially for fatigue properties in LPBF additive manufactured metal alloys due to rapid melting because of the high laser power used. Many solidification defects are reported [10-12] in LAM processed aluminum alloys. These defects are detrimental to fatigue properties of the alloy resulting in early crack initiation leading to premature fracture [13-17].

The published literature on S-N curve behavior of AlSi10Mg alloy in the as-built condition is limited, especially in terms of processing variables. So, the objective this investigation is, (i) to

Corresponding author: kvsudhakar@mtech.edu

evaluate the S-N curve behavior, and (ii) to investigate the fracture morphologies, as a function of energy density and build angle orientations.

Experimental Methods

LPBF additive manufacturing process

The powder had an average particle size distribution in the range 30 to 40 μm. In this investigation, the samples were produced using an EOS-M290-3D printer. Individual test specimens were produced on build plates at four different build angle orientations. The specimens produced at different build angle orientations had energy density values of 37.1 J/mm^3, 45.4 J/mm^3, and 49.9 J/mm^3. Samples were built at 0°, 30°, 60°, and 90° (as shown in Fig. 1) angles in relation to the build plate.

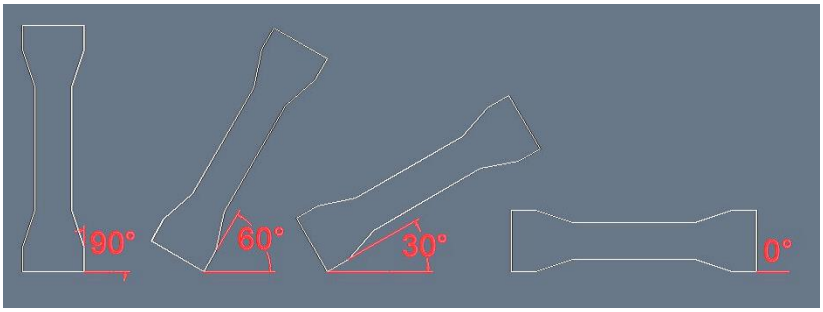

Fig. 1. Schematics of as-built specimen angle orientations

Fatigue tests

Fatigue tests were performed as per the ASTM standards E2948 and E1823. Rotating-bending *type* of high cycle fatigue test was conducted to generate S-N curve to determine the fatigue behavior. The test specimen design is based on the cantilever beam principle. All the rotating bending fatigue tests were performed using RBF-200 machine. Fatigue tests were conducted at a calculated starting stress value, based on the tensile test results of aluminum alloy specimens. The fractured specimens were used for fracture surface investigations.

Results and Discussion

Fatigue behavior of aluminum alloy

Based on the calculated bending moments, the continuous radius (to ensure that the maximum bending stresses are constant at all cross sections) specimens were subjected to zero mean load, since the loaded test specimens experience equal amounts of alternating tensile and compressive stresses. In this test, three specimens were tested for each value of specimen orientation and energy density. As per the ASTM standard, a maximum limit of 10^7 cycles was used to define the fatigue limit. The fatigue limit was determined when the specimen experienced no failure/fracture.

S-N Curves

Influence of specimen build angle orientations on fatigue

Fatigue behavior in terms of an S-N curve is demonstrated in Fig. 2.

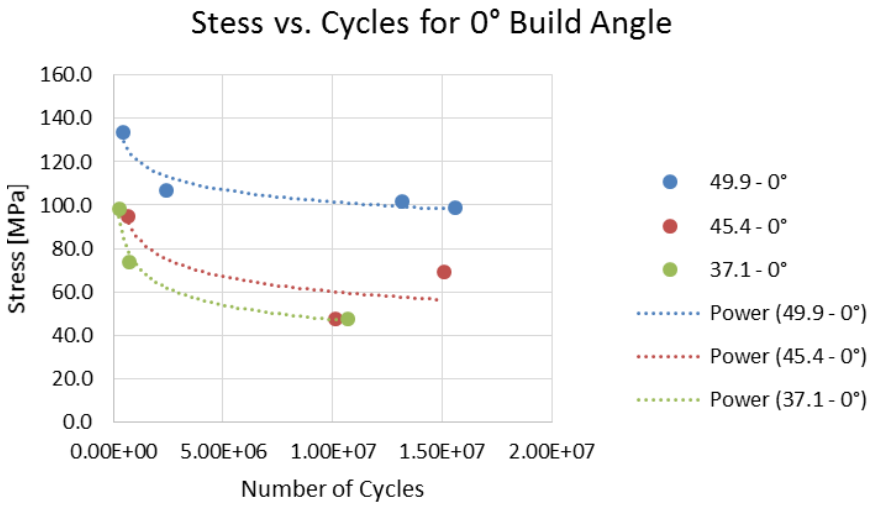

Fig. 2. Fatigue behavior for 0° build angle specimens at different energy densities

The fatigue limit increased (as revealed in Fig. 2) with the increase in energy density used in LPBF processing of aluminum alloy specimens. This is due to the fact that at higher energy densities, there is more heat available for the complete fusion of the metal powder layers. As a result, the specimens produced at relatively higher energy levels were completely bonded between layers in addition to being more homogeneous in terms of microstructure. The specimens produced at lower energy density were observed to be partially fused resulting in relatively more number of discontinuities.

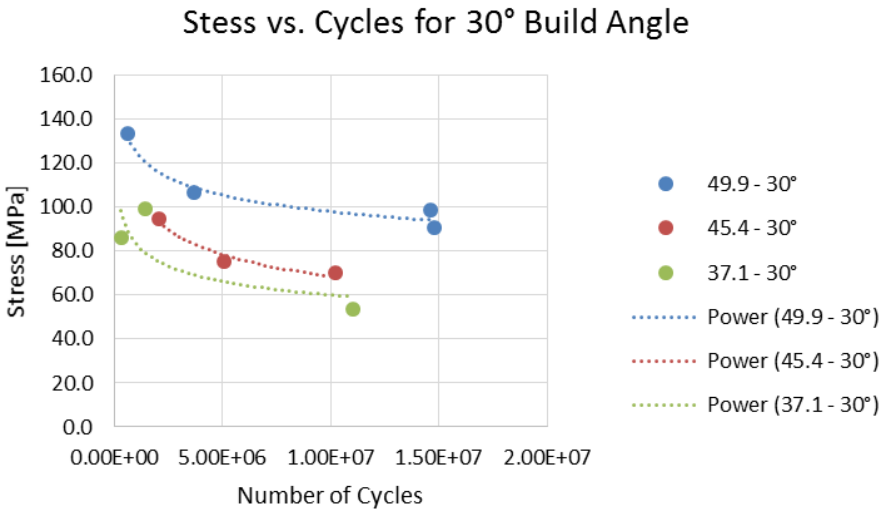

Fig. 3. Fatigue behavior for 30° build angle specimens at different energy densities

Fig. 3 demonstrates the fatigue curve for the 30° build angle oriented specimen. The trend of fatigue behavior is the same as that of the 0° build angle orientation.

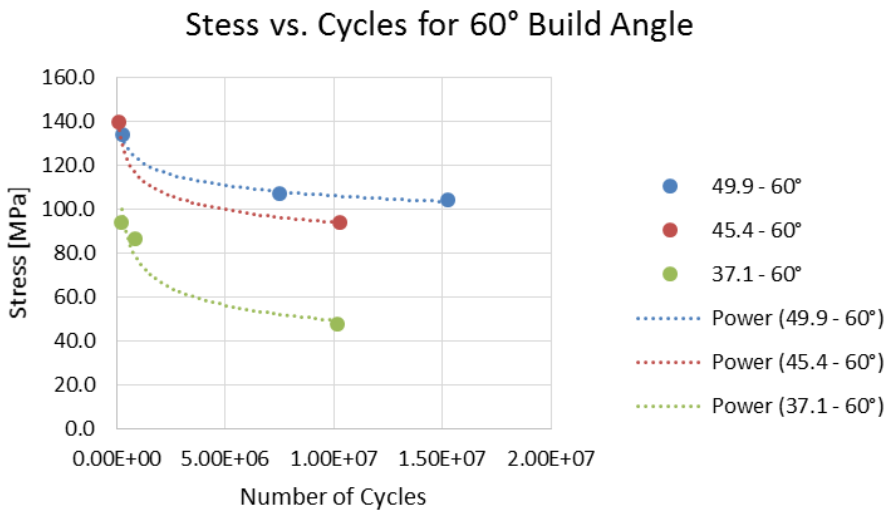

Fig. 4. Fatigue behavior for 60° build angle specimens at different energy densities

Figure 4 shows the fatigue curve for the 60° build angle oriented specimen. Fig. 5 shows the fatigue behavior of the specimen built at 90° angle orientation.

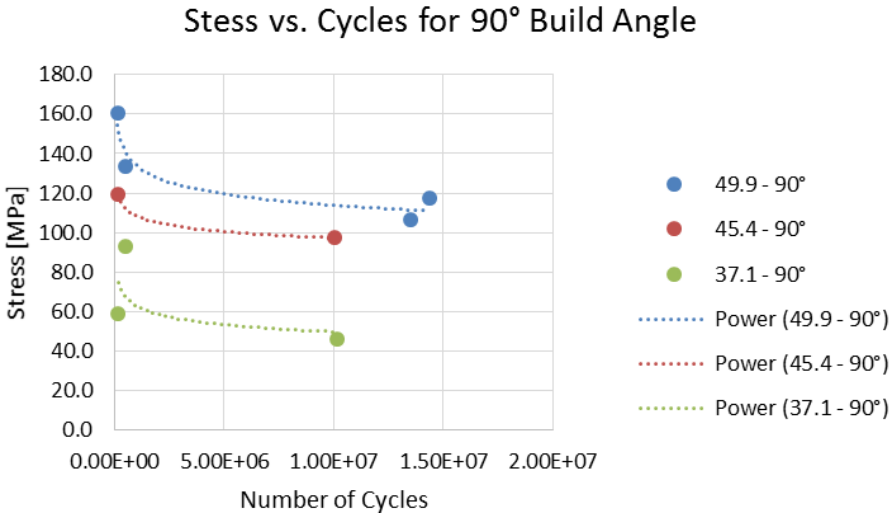

Fig. 5. Fatigue behavior for 90° build angle specimens at different energy densities

Fatigue behavior as a function of global energy density

From Fig. 5 and 6, it may be concluded that the 90° build angle specimens exhibited the highest fatigue life at 49.9 J/mm^3 energy density among all other combinations of build angles and energy densities. Again, this is as a result of the increased fusion between layers and more homogeneous microstructures. The trend of fatigue behavior is the same for all the specimen built at different angle orientations.

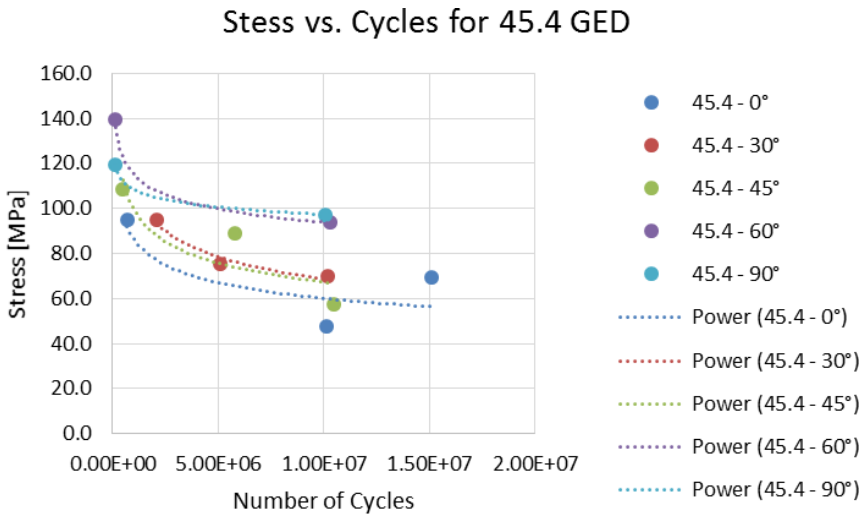

Fig. 6. Fatigue behavior for 45.4 J/mm3 energy density at various build angle specimens

Based on Fig. 6 and 7, it is clear seen that the best fatigue life was observed for the specimens produced with higher energy density. This is attributed to sufficient fusion between layers resulting from higher energy densities leading to improved bonding between the layers.

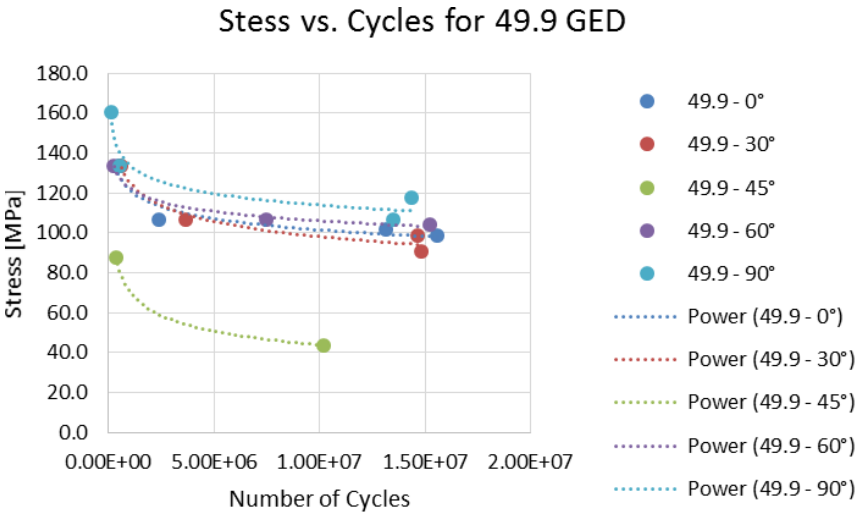

Fig. 7. Fatigue behavior for 49.9 J/mm3 energy density at various build angle specimens

Fractography features as a function of energy density and build angle orientation

Three fracture zones for fatigue fractured specimens (at energy density 49.9 J/mm^3 and 0° build angle) can be seen in a low magnification fractograph depicted in Fig. 8a Fig. 8b shows the crack initiation zone at a higher magnification showing the evidence of porosity and/or inclusions. The crack propagation region is relatively smooth and showing cleavages that are characteristics of a brittle fracture.

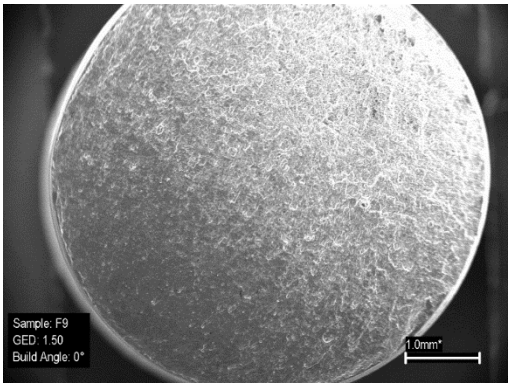

Fig. 8a. Fractograph of specimens with energy density 49.9 J/mm^3 and 0° specimen orientation

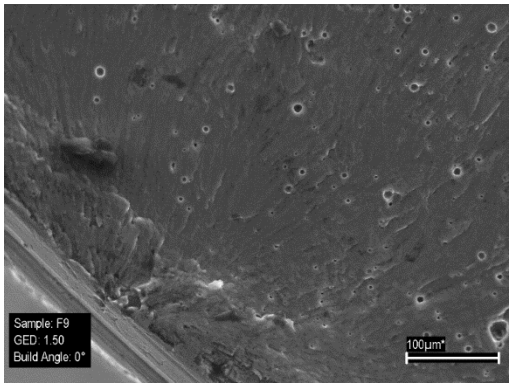

Fig. 8b. Fractograph of 8(a), showing crack initiation

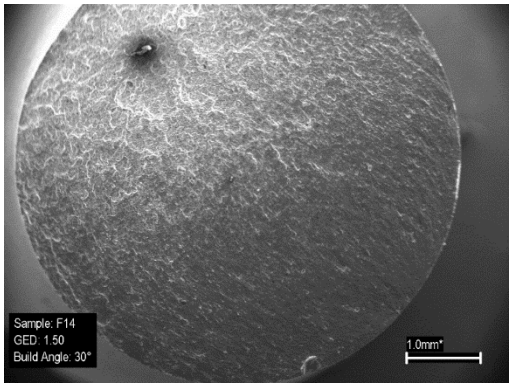

Fig. 9a. Fractograph of specimens with energy density 49.9 J/mm3 and 30° specimen orientation

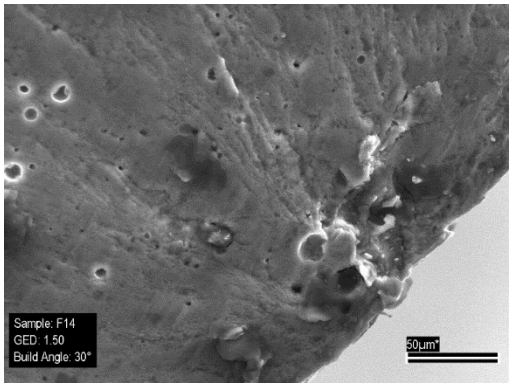

Fig. 9b. Fractograph of 9(a), showing crack initiation

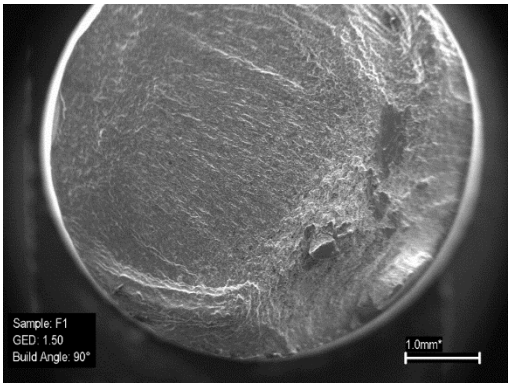

Fig. 10a. Fractograph of specimens with energy density 49.9 J/mm^3 and 90° specimen orientation

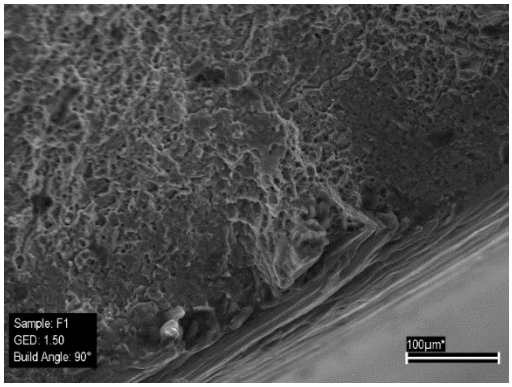

Fig. 10b. Fractograph of 10(a), showing crack initiation

Fractograph of the fatigue fractured specimen (49.9 J/mm^3 GED and 30° build angle) is shown in Fig. 9a (at low magnification). Fig. 9b clearly demonstrates the presence of porosity and unmelted particles, as the locations for crack initiation. The crack propagation region (Figure 9b) is flat and smooth, typical of a brittle mode of fracture.

Fracture surface features of all different regions of crack leading to final fracture is shown in Fig. 10a. Fig. 10b reveals the presence of partially fused powder particles. The crack propagation region depicting large amounts of voids, ductile ridges, and fibrous features that are typical of a ductile fracture can also be seen in Fig. 10b.

Conclusions

Aluminum alloy produced at 90° build angle exhibited higher fatigue strength/life in comparison to the rest of build angle orientations (0°, 30°, and 60°). More tortuous fatigue crack growth through well-bonded multiple build layers is the reason for improvement in fatigue life.

Higher fatigue strength/life was observed for the aluminum alloy specimens produced with higher energy density at 49.9 J/mm^3.

Fractography revealed that the fatigue cracks were initiated at locations containing inclusions, porosity, and unmelted/partially melted powder particles.

Fatigue fracture mode was predominantly ductile for specimens produced at higher energy density. This is attributed to relatively higher fusion between the layers and homogeneous microstructures at higher energy densities.

Acknowledgement

"Research was sponsored by the Army Research Laboratory and was accomplished under Cooperative Agreement Number W911NF-15-2-0020. The views and conclusions contained in this document are those of the authors and should not be interpreted as representing the official policies, either expressed or implied, of the Army Research Laboratory or the U.S. Government. The U.S. Government is authorized to reproduce and distribute reprints for Government purposes notwithstanding any copyright notation herein."

The authors wish to thank Mr. Gary Wyss, Senior Scientist, CAMP, for SEM analysis, and Ronda Coguill and Taylor Winsor for the support on fatigue tests. Thanks are also due to Dr. Bruce Madigan and Steven Keckler.

References

[1] W. E. Frazier, *Metal Additive Manufacturing: A Review*, **ASM International**, **23**, 2014, pp. 1917-1928.

[2] D. Herzog, V. Seyda, E. Wycisk and C. Emmelmann, *Addivie manufacturing of metals*, **Acta Materialia**, 2016, pp. 371-392.

[3] K. Kempen, L. Thijs, J. Van Humbeeck and J.-P. Kruth, *Processing AlSi10Mg by selective laser melting: parameter optimisation and material characterisation*, **Materials Science and Technology**, 2015, pp. 917-923.

[4] E. O. Olakanmi, R. F. Cochrane and K. W. Dalgrno, *A review on selective laser sintering/melting (SLS/SLM) of aluminum alloy powders: Processing, microstructure, and properties*, **Progress in Materials Science**, 2015, pp. 401-477.

[5] EOS GmbH - Electro Optical *Systems*, "EOS Aluminium AlSi10Mg," EOS GmbH - Electro Optical Systems, Krailling/München, 2018.

[6] N. T. Aboulkhair, I. Maskery, C. Tuck, I. Ashcroft and N. M. Everitt, *The microstructure and mechanical properites of selectively laser melted AlSi10Mg: The effect of a conventional T6-like heat treatment*, **Materials Science and Engineering A**, 2016, pp. 139-146.

[7] N. T. Aboulkhair, I. Maskery, C. Tuck, I. Ashcroft and N. M. Everitt, *The microstructure and mechanical properites of selectively laser melted AlSi10Mg: The effect of a*

conventional T6-like heat treatment, **Materials Science and Engineering A**, 2016, pp. 139-146.

[8] E. Brandl, U. Heckenberger, V. Holzinger and D. Buchbinder, *Additive manufactured AlSi10Mg samples using Selective Laser Melting (SLM): Microstructure, high cycle fatigue, and fracture behavior*, **Materials and Design**, 2012, pp. 159-169.

[9] C. Kammer, Alkuminum Taschenbuch Band 1, Düsseldort: Beuth, 2009.

[10] R. Li, J. Liu, Y. Shi, L. Wang, W. Jiang, *Balling behavior of stainless steel and nickel powder during selective laser melting process*, **International Journal of Advanced Manufacturing Technology**, 2012, 59 (9–12), pp. 1025-1035.

[11] W.E. King, H.D. Barth, V.M. Castillo, G.F. Gallegos, J.W. Gibbs, D.E. Hahn, C. Kamath, A.M. Rubenchik, *Observation of keyhole-mode laser melting in laser powder-bed fusion additive manufacturing*, **Journal of Materials Processing Technology**, **214 (12)**, 2014, pp. 2915-2925.

[12] Y. Liu, Y. Yang, S. Mai, D. Wang, C. Song, *Investigation into spatter behavior during selective laser melting of AISI 316L stainless steel powder*, **Materials Design**, **87,** 2015, pp. 797-806.

[13] E. Wycisk, A. Solbach, S. Siddique, D. Herzog, F. Walther, C. Emmelmann, *Effects of defects in laser additive manufactured Ti-6Al-4V on fatigue properties*, **Physics Procedia**, **56**, 2014, pp. 371-378.

[14] M. Akita, Y. Uematsu, T. Kakiuchi, M. Nakajima, R. Kawaguchi, Defect-dominated fatigue behavior in type 630 stainless steel fabricated by selective laser melting, **Materials Science & Engineering**, **A 666**, 2016, pp. 19-26.

[15] A. Yadollahi, N. Shamsaei, S.M. Thompson, A. Elwany, L. Bian, *Effects of building orientation and heat treatment on fatigue behavior of selective laser melted 17-4 PH stainless steel*, **International Journal of Fatigue**, **94,** 2017, pp. 218-235.

[16] E. Brandl, U. Heckenberger, V. Holzinger, D. Buchbinder, *Additive manufactured AlSi10Mg samples using Selective Laser Melting (SLM): microstructure, high cycle fatigue, and fracture behavior*, **Materials Design**, **34,** 2012, pp. 159-169.

[17] L. J. Suttey, *Evaluation of Metallurgical and Mechanical Properties of AlSi10Mg Produced by Selective Laser Melting*, **https://digitalcommons.mtech.edu**/grad_rsch/174, 2018, pp. 1-98.

Received: December 12, 2018
Accepted: February 10, 2019